JOURNAL OF THEORETICAL AND APPLIED MECHANICS
63, 1, pp. 131-149, Warsaw 2025
https://doi.org/10.15632/jtam-pl/195727

YAW FEEDBACK CONTROL OF ACTIVE STEERING VEHICLE BASED ON DIFFERENTIAL FLATNESS THEORY

Haiyan Qiang

Logistics Engineering College, Shanghai Maritime University, Shanghai, China and Key Laboratory of Railway Industry of Maglev Technology, Tongji University, Shanghai, China

Cheng Xiao, Hengyue Huang, Yichen Hai

Logistics Engineering College, Shanghai Maritime University, Shanghai, China

Yougang Sun

National Maglev Transportation Engineering R&D Center, Tongji University, Shanghai, China

e-mail: 1989yoga@tongji.edu.cn

In order to solve the problems of nonlinearity, underactuation and insufficient lateral stability of an active steering vehicle (ASV) in trajectory tracking tasks, a yaw feedback control strategy based on differential flatness theory is proposed in this paper. Firstly, the vehicle integrated monorail model is established, and the vehicle model is linearized by small angle approximation. Secondly, a suitable flat output is found to convert a complex vehicle model into a full drive system, and the flatness of the linear model is proved. Then, an equivalent form of the vehicle model is constructed based on the flat output and its derivatives, and a feedback controller based on the differential flat theory is designed to complete the trajectory tracking control through active steering and longitudinal motion. Finally, an ASV control simulation model is built in MATLAB/Simulink, and the simulation results show the effectiveness of the proposed control strategy under different maneuvering conditions.

Keywords: differential flatness; trajectory tracking; feedback control; underactuated system; lateral stability

1. Introduction

Active steering vehicles (ASVs) are poised to play a major role in the future of intelligent transportation. They have the potential to improve vehicle stability, enhance traffic efficiency and safety, and promote low-carbon transportation. With the integration of computer vision technology, sensor intelligent perception technology, Internet of Things (IoT) technology, and new control strategies (Ortiz *et al.*, 2023; Sun *et al.*, 2023; Luo *et al.*, 2022), the vehicle yaw control has made significant progress and has become a key research focus in modern land transportation. ASV yaw control can automatically track reference trajectories under varying speeds, complex road conditions, and uncertain disturbances, guaranteeing enhanced tracking accuracy and lateral stability.

Importantly, the differential flatness approach can be widely applied in the transportation sector, as shown in Fig. 1, which includes self-driving passenger cars, self-driving buses, intelligent express delivery cars, port container driverless transport vehicles, and engineering transport vehicles, among others.

In recent years, the intelligent vehicle trajectory tracking control has attracted attention of researchers worldwidely. Most of these studies focus on tracking accuracy, lateral stability, and control methods, yielding substantial results (Yu *et al.*, 2021; Sun *et al.*, 2024; Yang *et al.*, 2021;

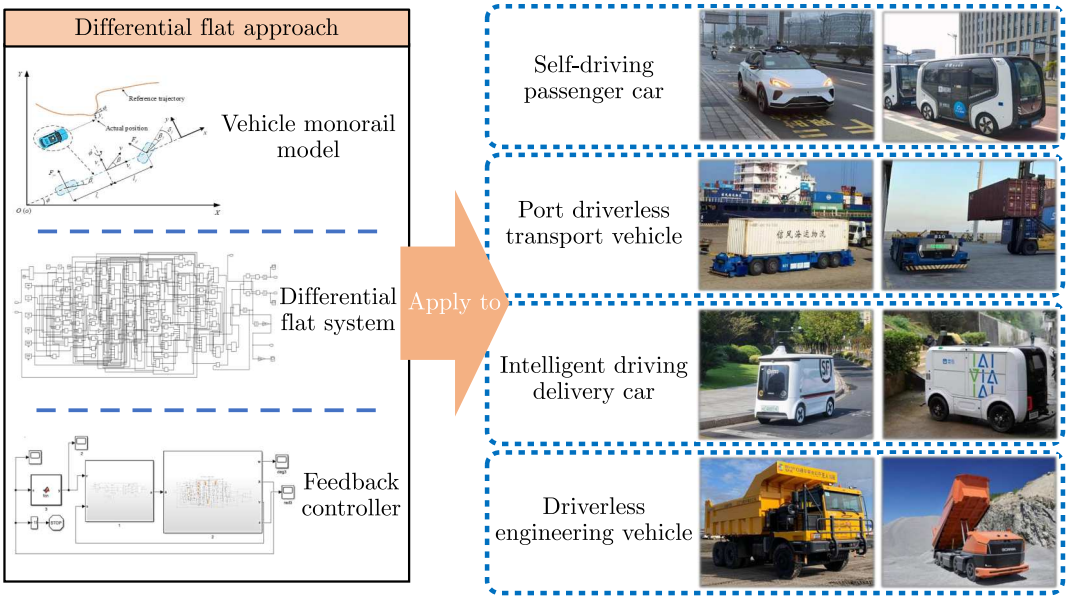

Fig. 1. Possible application areas for the differential flatness approach

Sun *et al.*, 2023). Wang and Sun (2023) designed a linear quadratic regulator combining feedforward and feedback, adopting a fuzzy control algorithm and cosine similarity updating mechanism to quickly adjust weight values, thereby improving vehicle tracking accuracy and computational efficiency. Rokonuzzaman (2021) developed a dynamic model predictive controller based on neural networks combined with the big data system of intelligent vehicles, enhancing the accuracy of vehicle models, and tracking performance. Bai (2019) introduced a nonlinear model predictive controller for mining vehicles, which effectively ensured stable and accurate tracking at high longitudinal speeds. Mata (2019) proposed a tube-based robust model predictive control method for vehicle path tracking, considering dynamic differences between the actual vehicle and the mathematical model and strict constraints on control signals and lateral errors to ensure tracking accuracy and driving comfort. Kang (2022) suggested an improved active disturbance rejection control method, applying a new continuous nonlinear function to the extended state observer, optimally allocating yaw moment to the four wheels to achieve differential control, enhancing tracking effect and anti-disturbance robustness. Guerrero (2023) designed a generalized super-twisting algorithm controller to address the disturbance problem of underwater vehicles, conducting stability analysis under different disturbances, with simulation results showing good performance.

It is evident that considering both the lateral displacement and yaw angle response in trajectory tracking research is crucial for improving vehicle tracking performance. However, many studies overlook the underactuated characters of vehicle systems, with few focusing on underactuated vehicle systems. Most research on underactuation are focused on the field of foot robots, robotic arms, aircraft, and surface vehicles, etc. To achieve more accurate control of the lateral displacement and yaw angle response, differential flatness theory and feedback control can be applied to address the underactuated vehicle system problem.

Fliess (1995) introduced a system equivalent to a linear system through special feedback, identified as a differentially flat system. Using crane motion planning as an example, it was demonstrated that the input of a differentially flat system could be expressed through a combination of the output and its derivatives, which significantly reduced complex integral operations. This illustrates those issues of uncontrollability, nonlinearity, and underactuation can be resolved using the properties of differential flatness theory. Huang (2019) proposed an active disturbance rejection control method based on differential flatness for nonlinear systems with periodic and

aperiodic characteristics, identifying total system disturbances, selecting appropriate observers, and employing the fruit fly optimization algorithm to determine controller parameters. The effectiveness of the proposed method was validated through simulation. Elmi (2013) established a three-degree-of-freedom vehicle model, designed a robust linear quadratic regulator, and performed simulation analysis across a wide range of vehicle speeds and tire characteristics, demonstrating that the proposed controller ensured robust stability under varying conditions. Aschemann *et al.* (2008) combined differential flatness and sliding mode control to enhance error dynamics stability for unmodeled aerodynamic mechanisms. Differential flatness theory can also resolve system underactuation issues, as illustrated by Zhuang (2010) who applied differential flatness to achieve optimal motion planning for non-axisymmetrical spacecraft.

This paper focuses on the yaw control strategy of single-input, multiple-output underactuated vehicles in trajectory tracking tasks. The main contributions are summarized as follows:

- The differential flatness of an integrated monorail vehicle model is demonstrated, and the assumed differential flatness output is validated.
- Based on the differential flatness and flat output, the equivalent system form is derived, representing the system with the differential flat output and its derivatives, thus solving the underactuation problem.
- A feedback controller based on differential flatness theory is designed, providing high control accuracy and robust performance.

The organizational structure of this paper is as follows: In Section 2, an integrated monorail model of ASV is built, combining vehicle kinematics and dynamics. In Section 3, the validity of the assumed flat output and the differential flatness of the system are proved. In Section 4, the original system is transformed into an equivalent system represented by the differential flat output and its derivatives, and a feedback controller based on differential flatness theory is designed. In Section 5, simulations on ASV in Simulink demonstrate the superiority of the proposed strategy. Section 6 concludes the paper.

2. Vehicle integrated monorail model

ASV is an underactuated integrated system with high complexity, strong nonlinearity, and uncertainties. In trajectory tracking tasks, its dynamic model is characterized by numerous constraints and high nonlinearity, making accurate modeling challenging (Wang *et al.*, 2022). Therefore, in this Section, the vehicle kinematics and dynamics are combined to establish an integrated monorail model of an active steering vehicle.

To align with practical scenarios and facilitate subsequent research, the important characteristics of the lateral and yaw direction of the vehicle are the focus of this research. The following assumptions are made during the model establishment process:

- The influence of air resistance, tire changes, and the suspension system is ignored.
- Vertical, tumbling, and pitching movements are disregarded.
- The tire slip angle is small, and the tire lateral force is proportional to the slip angle.
- The road adhesion state and vehicle driving conditions are optimal.
- Active steering is applied to the front wheels of the vehicle.

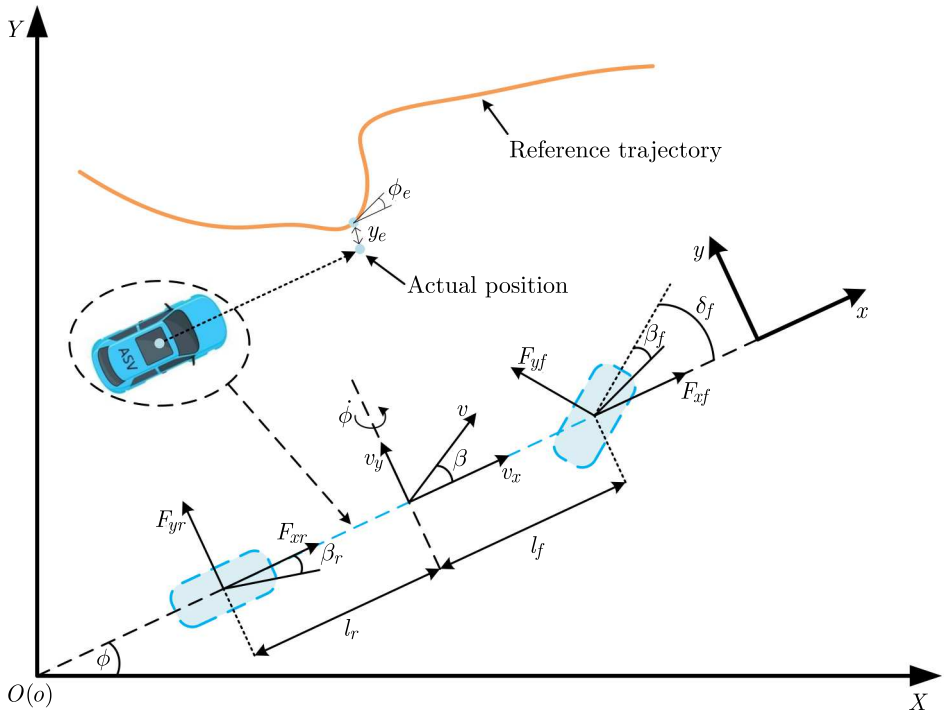

Fig. 2. Vehicle monorail model

Based on the assumptions above, a vehicle model, which is simplified to a monorail model, by considering the similar motion and dynamic characteristics exhibited for both sides of the vehicle, is established, as shown in Fig. 2.

In Fig. 2, XOY denotes the global coordinate system of the earth, xoy is the vehicle centroid coordinate system, y_e is the lateral deviation, ϕ_e is the deviation of yaw angle. The kinematic model considering the lateral and yaw of the vehicle can be expressed as follows

$$\Delta\dot{Y} = v_x \sin\phi + v_y \cos\phi \qquad \dot{\phi} = w \tag{2.1}$$

where v_x and v_y represent longitudinal velocity and transverse velocity, respectively, ϕ indicates the vehicle yaw angle, w indicates the yaw angular speed of the vehicle.

According to Fig. 2, the dynamic model considering the lateral and yaw of the vehicle can be expressed as follows

$$F_{yf}\cos\delta_f + F_{yr} = m(\dot{v}_y + v_x\dot{\phi}) \qquad l_f F_{yf}\cos\delta_f - l_r F_{yr} = I\ddot{\phi} \tag{2.2}$$

where F_{yf} and F_{yr}, respectively, represent the lateral force of the road on the front and rear wheels of the vehicle, l_f and l_r represent the distance from the center of the front and rear wheels to the center of mass, respectively. δ_f represents the active steering angle of the vehicle, m represents vehicle mass, I represents the yaw moment of inertia of the vehicle.

Considering the lateral force generated by the interactions among the front and rear wheels and the ground, combined with the assumptions made in the process of vehicle model building, it can be considered that the lateral force is proportional to the side yaw angle, so the lateral force and side yaw angle can be expressed as

$$\begin{aligned} &F_{yf} = -C_{kf}\beta_f \qquad F_{yr} = -C_{kr}\beta_r \\ &\beta_f \approx (v_y + wl_f - \delta_f v_x)/v_x \qquad \beta_r \approx (v_y - wl_r)/v_x \end{aligned} \tag{2.3}$$

where C_{kf} and C_{kr} represent the lateral stiffness of the front and rear wheels, respectively, β_f and β_r represent the front and rear wheel side angles.

Generally, a small angle approximation is carried out for the vehicle under normal driving conditions (Wang *et al.*, 2014), namely: $\cos\delta_f \approx 1$, $\sin\phi \approx \phi$, $\cos\phi \approx 1$. Equations (2.1)–(2.3) are combined to obtain the vehicle integrated monorail model equation

$$\begin{aligned}
&\Delta\dot{Y} = v_x\phi + v_y \qquad \dot{\phi} = w \\
&\dot{v}_y = -v_x\dot{\phi} + 2[C_{kf}(\delta_f v_x - wl_f - v_y) + C_{kr}(wl_r - v_y)]/v_x m \\
&\dot{w} = 2[l_f C_{kf}(\delta_f v_x - wl_f - v_y) - l_r C_{kr}(wl_r - v_y)]/v_x I
\end{aligned} \tag{2.4}$$

In order to facilitate subsequent derivation and research, the vehicle model equation is simplified, and the relevant parameter combinations are replaced by simple equivalent characters, and the simplified vehicle model equation can be obtained

$$\begin{aligned}
&\Delta\dot{Y} = g\phi + v_y \qquad \dot{\phi} = w \\
&\dot{v}_y = eh + (av_y + bw - g^2 w)/g \qquad \dot{w} = fh + (cv_y + dw)/g
\end{aligned} \tag{2.5}$$

where

$$\begin{aligned}
a &= -2(C_{kf} + C_{kr})/m \qquad e = 2C_{kf}/m \\
b &= 2(C_{kr}l_r - C_{kf}l_f)/m \qquad f = 2C_{kf}l_f/I \\
c &= 2(C_{kr}l_r - C_{kf}l_f)/I \qquad g = v_x \\
d &= -2(C_{kr}l_r + C_{kf}l_f)/I \qquad h = \delta_f
\end{aligned}$$

Assuming $x_1 = \Delta Y$, $x_2 = v_y$, $x_3 = \phi$, $x_4 = w$, and $x = \begin{bmatrix} x_1 & x_2 & x_3 & x_4 \end{bmatrix}^{\mathrm{T}}$ is regarded as the system state variable, $h = \delta_f$ as the control input, and y is defined as the output after system operation, then the vehicle model equation above can be converted into the state space equation

$$\dot{x} = \mathbf{A}_0 x + \mathbf{B}_0 h \qquad y = \mathbf{C}_0 x \qquad x \in R^4 \tag{2.6}$$

where

$$\mathbf{A}_0 = \begin{bmatrix} 0 & 1 & g & 0 \\ 0 & a/g & 0 & (b-g^2)/g \\ 0 & 0 & 0 & 1 \\ 0 & c/g & 0 & d/g \end{bmatrix} \qquad \mathbf{B}_0 = \begin{bmatrix} 0 \\ e \\ 0 \\ f \end{bmatrix} \qquad \mathbf{C}_0 = \begin{bmatrix} 1 & 0 & 0 & 0 \\ 0 & 0 & 1 & 0 \end{bmatrix}$$

3. Differential flat system construction and output

3.1. Differential flatness theory

For a system $\dot{x} = \kappa_1(x, h)$, κ_1 represents a smooth continuous function, $x \in R^{n_1}$, $h \in R^{n_2}$. According to the property of differential flatness, a set of flat output $P \in R^{n_2}$ can be found to represent a combination of system state variables, control variables and their derivatives, and both the system state variables and control variables can be represented by the flat output and its derivatives (Menhour *et al.*, 2014). The system can be regarded as a system based on differential flatness theory.

The general form of a flat output is as follows

$$P = \boldsymbol{\xi}(x, h, \dot{h}, ..., h^{(i)}) \tag{3.1}$$

where $\boldsymbol{\xi}$ represents a smooth vector function.

The general form of the system state variable and control variable composed of the flat output and its derivatives is as follows

$$x = \boldsymbol{\psi}_x(P, \dot{P}, ..., P^{(i)}) \qquad h = \boldsymbol{\psi}_h(P, \dot{P}, ..., P^{(i)}) \quad x \in R^{n_1} \quad h \in R^{n_2} \quad P \in R^{n_2} \tag{3.2}$$

where $\boldsymbol{\psi}_x$, $\boldsymbol{\psi}_h$ both represent smooth vector functions.

3.2. Differential flatness output and flatness proof

If a linear system is controllable, it has differential flatness and can find the corresponding flat output. The combination of the flat output of a controllable linear system, the inverse of the Kalman controllability discriminant matrix and the system state variable can represent the corresponding flat output (Sira-Ramirez *et al.*, 2004; Xia *et al.*, 2016). It can be described more accurately by a linear system

$$\dot{x} = Ax + Bh \qquad y = Cx \qquad x \in R^n \tag{3.3}$$

Based on the above system, a general form of the flat output can be found

$$\mathbf{P}_0 = \begin{bmatrix} 0 & 0 & 0 & ... & 1 \end{bmatrix} \begin{bmatrix} \mathbf{B} & \mathbf{AB} & \mathbf{A}^2\mathbf{B} & ... & \mathbf{A}^{n-1}\mathbf{B} \end{bmatrix}^{-1} x \tag{3.4}$$

where matrices $\mathbf{A}_0$ and $\mathbf{B}_0$ are relatively fixed values derived from the model, the system state variable x changes with the input value, so the flat output $\mathbf{P}_0$ mainly depends on the state variable of the system.

For active steering vehicle system (2.6), according to the controllability discrimination theory, its controllability matrix is shown in (3.5). By using data analysis software to calculate $\text{rank}\,(\mathbf{K}_0) = 4$, that is: matrix $\mathbf{K}_0$ is in a state of full rank. Therefore, system (2.6) is judged to be controllable. The matrix $\mathbf{K}_0$ looks like this

$$\begin{aligned} \mathbf{K}_0 &= \begin{bmatrix} \mathbf{B}_0 & \mathbf{A}_0\mathbf{B}_0 & \mathbf{A}_0^2\mathbf{B}_0 & \mathbf{A}_0^3\mathbf{B}_0 \end{bmatrix} \\ &= \begin{bmatrix} 0 & e & (ae+bf)g^{-1} & (ea^2+ebc+fab+fbd)g^{-2}-fa \\ e & (ae+fb)g^{-1}-fg & (ea^2+eb+fab-bd)g^{-2}-ec-fa+d & \Delta_{24} \\ 0 & f & (ce+df)g^{-1} & (fd^2+fcb+eac+ecd)g^{-2}-cf \\ f & (ce+df)g^{-1} & (fd^2+bcf+ace+cde)g^{-2}-cf & \Delta_{44} \end{bmatrix} \end{aligned} \tag{3.5}$$

where

$$\begin{aligned} \Delta_{24} &= -e(ca+d)(g^{-1}-bg^{-3}) - a(a^2g^{-3} - c(g^{-1}-bg^{-3})) \\ &\quad - f((a^2g^{-2}-c+bcg^{-2})(g-bg^{-1}) + (a+1)dg^{-1} - (a+1)bdg^{-3}) \\ \Delta_{44} &= ce((bc+d^2)g^{-3} - cg^{-1}) + ae(a+d)cg^{-3} \\ &\quad - ef((a+d)cg^{-3}(1-bg^{-2}) - (bcd+d^3)g^{-4} + cdg^{-2}) \end{aligned}$$

When an active steering vehicle performs a trajectory tracking task, its system outputs are ΔY and ϕ, which are related to the value of matrix $\mathbf{C}_0$. It can be seen from (3.4) that the flat output is not affected by matrix $\mathbf{C}_0$, and the differential flat system is relatively independent, so the differential flat theory can be used here to analyze the system. In order to make the subsequent equations and derivations more concise, according to subsequent analysis and derivation, $ce^2 + f^2(g^2-b) + (d-a)ef$ is set to G and $0.001(ce-af)$ is set to u in advance, and u is set as a constant which is not 0. Obviously, if $\mathbf{P}_0$ is valid, then $u\mathbf{P}_0$ can also be expressed as a set of flat outputs, so the assumed flat outputs are

$$P = u\mathbf{P}_0 = 0.001u\begin{bmatrix} 0 & 0 & 0 & 1 \end{bmatrix}\mathbf{K}_0^{-1}x \tag{3.6}$$

After expansion

$$P = \alpha_1 x_1 + \alpha_2 x_2 + \alpha_3 x_3 + \alpha_4 x_4 \tag{3.7}$$

where

$$\begin{aligned}
&\alpha_1 = 0.001 \qquad \alpha_2 = 0.001fg(bf^2 - ce^2 + aef - def)/(afG - ceG)\\
&\alpha_3 = 0.001(bf - de)/(af - ce)\\
&\alpha_4 = 0.001eg(ce^2 - aef - bf^2 + def)/(afG - ceG)
\end{aligned}$$

To get the differential flat output of the state variable, take the derivative of P

$$\begin{aligned}
\dot{P} &= \beta_1 x_1 + \beta_2 x_2 + \beta_3 x_3 + \beta_4 x_4 + \beta_5 h\\
\ddot{P} &= \eta_1 x_1 + \eta_2 x_2 + \eta_3 x_3 + \eta_4 x_4 + \eta_5 h\\
P^{(3)} &= \lambda_1 x_1 + \lambda_2 x_2 + \lambda_3 x_3 + \lambda_4 x_4 + \lambda_5 h
\end{aligned} \tag{3.8}$$

where

$$\begin{aligned}
&\beta_1 = \beta_5 = 0 \qquad \beta_3 = 0.001g\\
&\beta_2 = 0.001f^2g^2/G \qquad \beta_4 = -0.001efg^2/G\\
&\eta_1 = \eta_3 = \eta_5 = 0 \qquad \lambda_1 = \lambda_3 = \lambda_5 = 0\\
&\eta_2 = 0.001fg(af - ce)/G \qquad \lambda_2 = 0.001(af - ce)^2/G\\
&\eta_4 = 0.001eg(ce - af)/G \qquad \lambda_4 = 0.001(ce - af)(fg^2 - bf + de)/G
\end{aligned}$$

From (3.7) we know that $\beta_5 = \eta_5 = \lambda_5 = 0$, so the state variable x can be represented by a combination of the flat output P and its derivatives $\dot{P}$, $\ddot{P}$, $P^{(3)}$, and by combining (3.6) and (3.7), we get

$$x = \begin{bmatrix} x_1 \\ x_2 \\ x_3 \\ x_4 \end{bmatrix} = \begin{bmatrix} \gamma_1 P + \gamma_2 \dot{P} + \gamma_3 \ddot{P} + \gamma_4 P^{(3)} \\ \mu_1 P + \mu_2 \dot{P} + \mu_3 \ddot{P} + \mu_4 P^{(3)} \\ \sigma_1 P + \sigma_2 \dot{P} + \sigma_3 \ddot{P} + \sigma_4 P^{(3)} \\ \tau_1 P + \tau_2 \dot{P} + \tau_3 \ddot{P} + \tau_4 P^{(3)} \end{bmatrix} \tag{3.9}$$

where

$$\begin{aligned}
&\gamma_1 = 1000 \qquad \gamma_3 = 1000e(ce - af)\\
&\gamma_2 = 1000(abf^2 - cde^2 + adef + bcef)/g \qquad \gamma_4 = 0\\
&\sigma_1 = \sigma_4 = 0 \qquad \sigma_2 = 1000/g \qquad \sigma_3 = 1000f/(ce - af)\\
&\mu_1 = \mu_2 = 0 \qquad \mu_3 = 1000(fg^2 - bf + de)/(afgG^2 - cegG^2)\\
&\mu_4 = 1000e(ce - af)/G^2\\
&\tau_1 = \tau_2 = 0 \qquad \tau_3 = 1000/(gG^2) \qquad \tau_4 = 1000f/(ceG^2 - afG^2)
\end{aligned}$$

Since the coefficients controlling the input amount h in $\dot{P}$, $\ddot{P}$, $P^{(3)}$ are all 0, the output expression of h cannot be flat, so it is necessary to obtain a higher derivative. From system (2.6), $\kappa_2(x, \dot{x}) = h$ can be obtained, and κ_2 represents a smooth continuous function. At this time, the fourth derivative of P is obtained

$$P^{(4)} = \varepsilon_1 x_1 + \varepsilon_2 x_2 + \varepsilon_3 x_3 + \varepsilon_4 x_4 + \varepsilon_5 h \tag{3.10}$$

where

$$\varepsilon_1 = \varepsilon_3 = 0 \qquad \varepsilon_2 = 0.001(ce - af)(ace - fa^2 + cfg^2 - bcf + ced)/(gG)$$
$$\varepsilon_4 = 0.001(ce - af)(ed^2 - abf + bce - bdf + afg^2 - ceg^2 + dfg^2)/(gG)$$
$$\varepsilon_5 = 0.001(ce - af)$$

From (3.10) we know that $\varepsilon_5 \neq 0$, so the control input h can be represented by the flat output and its derivatives, and by combining (3.7), (3.8), (3.9) and (3.10), we can get

$$h = \frac{(a+d)P^{(3)}}{gGu} - \frac{b\ddot{P}}{u} - \frac{(ad-bc)\ddot{P}}{g^2G^2u} - P^{(4)} \tag{3.11}$$

It is proved by (3.5), (3.9) and (3.11) that the differential flatness of system (2.6) is established and that the assumed output in (3.6) is indeed flat, that is, the state variables and control input variables of the system can be represented by the flat output and its finite derivatives, and the system has flatness.

4. Yaw feedback control strategy based on differential flatness theory

The equivalent system of (2.6) is established based on the differential flatness theory, assuming $\chi = [\ \chi_1 \quad \chi_2 \quad \chi_3 \quad \chi_4\ ]^{\mathrm{T}}$ and $\chi_1 = P$, $\chi_2 = \dot{P}$, $\chi_3 = \ddot{P}$, $\chi_4 = P^{(3)}$, the equivalent system can be obtained as follows

$$\dot{\chi} = \mathbf{A}_1\chi + \mathbf{B}_1 h_p \qquad y = \mathbf{C}_1\chi \tag{4.1}$$

where

$$\mathbf{A}_1 = \begin{bmatrix} 0 & 1 & 0 & 0 \\ 0 & 0 & 1 & 0 \\ 0 & 0 & 0 & 1 \\ 0 & 0 & (bc - ad - bg^2G^2)/(g^2G^2) & (a+d)/(gG) \end{bmatrix}$$

$$\mathbf{B}_1 = \begin{bmatrix} 0 \\ 0 \\ 0 \\ (af - ce)/1000 \end{bmatrix} \qquad \mathbf{C}_1 = \begin{bmatrix} 1 & 0 & 0 & 0 \end{bmatrix}$$

It can be assumed from (4.1) that $\kappa_3 = \dot{\chi}_4 - 0.001(af - ce)h$, so that the objective function can be tracked by controlling the differential flat output function to solve the system underdrive problem of ASV in trajectory tracking control.

In the feedback controller on the differential flatness (FCDF) control strategy, according to the target state variable x_p and the target control input variable h_p obtained from the differential flatness theory, the deviation system with $z_1 = x_1 - x_{p1}$, $z_2 = x_2 - x_{p2}$, $z_3 = x_3 - x_{p3}$, $z_4 = x_4 - x_{p4}$ as the state variable and $h_z = h - h_p$ as the control input variable is constructed.

$$x_p = \begin{bmatrix} x_{p1} \\ x_{p2} \\ x_{p3} \\ x_{p4} \end{bmatrix} = \begin{bmatrix} \kappa_4(\chi_1, \chi_2, \chi_3, \chi_4) \\ \kappa_5(\chi_1, \chi_2, \chi_3, \chi_4) \\ \kappa_6(\chi_1, \chi_2, \chi_3, \chi_4) \\ \kappa_7(\chi_1, \chi_2, \chi_3, \chi_4) \end{bmatrix} \qquad h_p = \kappa_8(\chi_1, \chi_2, \chi_3, \chi_4, \dot{\chi}_4)$$

where κ_i $(i = 4, 5, 6, 7, 8)$ is a smooth vector function.

Considering the deviation between the target value and the actual value of the state variable, the deviation of each state variable is substituted into the expression of the system state variable,

and the deviation expression of the vehicle system state variable can be obtained by combining system (2.6)

$$\begin{aligned} \dot{z}_1 &= gz_3 + z_2 \qquad \dot{z}_2 = (a/g)z_2 + (b - g^2)z_4/g + eh_z \\ \dot{z}_3 &= z_4 \qquad \dot{z}_4 = (c/g)z_2 + (d/g)z_4 + fh_z \end{aligned} \tag{4.2}$$

The forward Euler method is used for discretization

$$\begin{aligned} z_1(k+1) &= z_1(k) + T(gz_3(k) + z_2(k)) \\ z_2(k+1) &= z_2(k) + T((a/g)z_2(k) + (b - g^2)z_4(k)/g + eh_z(k)) \\ z_3(k+1) &= z_3(k) + Tz_4(k) \\ z_4(k+1) &= z_4(k) + T((c/g)z_2(k) + (d/g)z_4(k) + fh_z(k)) \end{aligned} \tag{4.3}$$

where T indicates the sampling time, which is 0.05 seconds in this numerical study, and k indicates the sampling order.

Assuming $z(k) = [\ z_1(k) \quad z_2(k) \quad z_3(k) \quad z_4(k)\ ]^{\mathrm{T}}$, the new discrete time-varying deviation system obtained by combining (4.2) and (4.3)

$$z(k+1) = \mathbf{A}_2 z(k) + \mathbf{B}_2 h_z(k) \tag{4.4}$$

where

$$\mathbf{A}_2 = \begin{bmatrix} 1 & T & gT & 0 \\ 0 & 1 + (a/g)T & 0 & (b - g^2)T/g \\ 0 & 0 & 1 & T \\ 0 & (c/g)T & 0 & 1 + (d/g)T \end{bmatrix} \qquad \mathbf{B}_2 = \begin{bmatrix} 0 \\ eT \\ 0 \\ fT \end{bmatrix}$$

A state feedback controller $h_z(k) = R(k)z(k)$ can be designed to stabilize the control deviation system approaching zero, then the corresponding system can be expressed as

$$z(k+1) = [\mathbf{A}_2(k, k+1) + \mathbf{B}_2(k, k+1)R(k)]\, z(k) \tag{4.5}$$

In the infinite time domain, the performance index of feedback control based on differential flatness is designed as H, satisfying the following expression

$$H_\infty(k) = \sum_{k=0}^{\infty} z^{\mathrm{T}}(k)\mathbf{M}z(k) + \sum_{k=0}^{\infty} h_z^{\mathrm{T}}(k)\mathbf{N}h_z(k) \tag{4.6}$$

where $\mathbf{M} = \mathrm{diag}\,(m_1, m_2, m_3, m_4)$, $\mathbf{N} = [n]$, both are weight matrices.

According to the Riccati algebraic equation, where Q is a positive definite solution of the equation and satisfies the following expression

$$\mathbf{M} + \mathbf{A}_1^{\mathrm{T}} Q \mathbf{A}_1 - \mathbf{A}_1^{\mathrm{T}} Q \mathbf{B}_1 (\mathbf{N} + \mathbf{B}_1^{\mathrm{T}} Q \mathbf{B}_1)^{-1} \mathbf{B}_1^{\mathrm{T}} Q \mathbf{A}_1 - Q = 0 \tag{4.7}$$

State feedback gain R satisfies the following expression

$$R = -(\mathbf{N} + \mathbf{B}_1^{\mathrm{T}} Q \mathbf{B}_1) \mathbf{B}_1^{\mathrm{T}} Q \mathbf{A}_1 \tag{4.8}$$

According to the vehicle monorail model, the reference active steering angle is $\delta_r = \arctan((l_f + l_r)(1 + \dot{y}^2)^{3/2} \big/ |\ddot{y}|)$, and the final control law of the vehicle actual active steering angle under the FCDF control strategy is

$$\delta_f = \delta_r + h_z(k) \tag{4.9}$$

Table 1. Vehicle parameters

Symbol	Meaning	Numerical value
m	Vehicle mass	1280 kg
l_f	Distance from center of mass to center of front wheel	1.2 m
l_r	Distance from center of mass to center of rear wheel	1.26 m
C_{kf}	Front wheel side stiffness	61000 N/rad
C_{kr}	Rear wheel side stiffness	61000 N/rad
I	Yaw moment of inertia	1630 kg·m^2

5. Simulation and analysis

To verify the effectiveness of the yaw feedback control strategy based on differential flatness, a vehicle model using differential flatness theory was established in MATLAB/Simulink. The parameters of the test vehicle are shown in Table 1.

During the path tracking process, it is assumed that the longitudinal speed of the vehicle is constant at $v_x = 50\,\text{km/h}$. In order to simulate the trajectory of a real road vehicle, the curvature of the curve is usually between 0.005 and 0.0001 according to highway engineering technical standards, so the smooth trajectory design helps the vehicle maintain a stable dynamic response when it is tested. Lane change and overtaking condition tests were conducted. The track reference value and yaw angle reference value for these conditions are shown in Figs. 3 and 4, respectively.

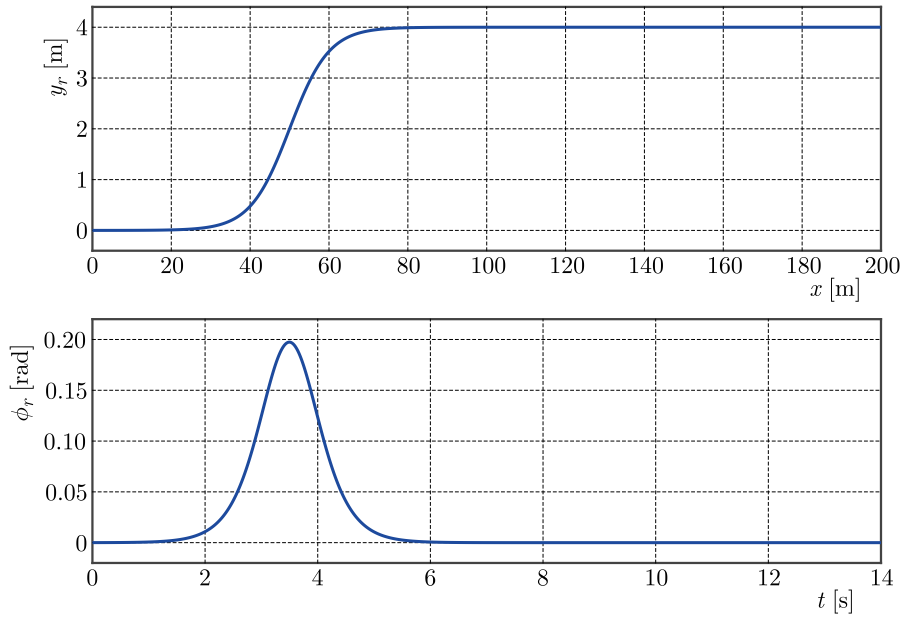

Fig. 3. Reference track and reference yaw angle under lane change conditions

The designed FCDF controls the vehicle for active steering, ensuring that the actual driving trajectory of the vehicle closely follows the reference trajectory. It also minimizes the deviation between the vehicle yaw angle and the reference value, ensuring good tracking accuracy and lateral stability. This Section demonstrates the superiority of the FCDF control strategy by comparing and analyzing its tracking effect against the PID control strategy.

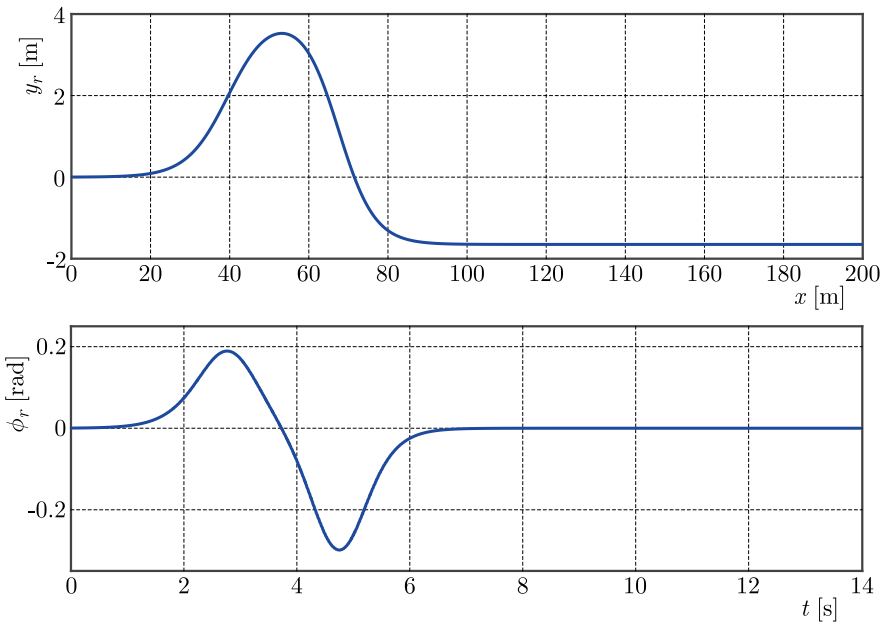

Fig. 4. Reference track and reference yaw angle under overtaking conditions

5.1. Lane change condition test

The lane change condition test verifies the track tracking effect and lateral performance of the vehicle under normal tracking and its response performance under external a random excitation.

Figure 5 shows the response curve of the trajectory tracking effect and lateral deviation. Simulation results indicate that the maximum absolute lateral deviation under PID and FCDF control is 0.1702 m and 0.1006 m, respectively. Compared to PID, the deviation amplitude under FCDF control is smaller, within the range of $(-0.1006,\ 0.0022)$ m. The linear section tracking accuracy is higher with minimal lateral deviation in the curved section. The final deviation convergence rate is 3.4 seconds faster than that for PID.

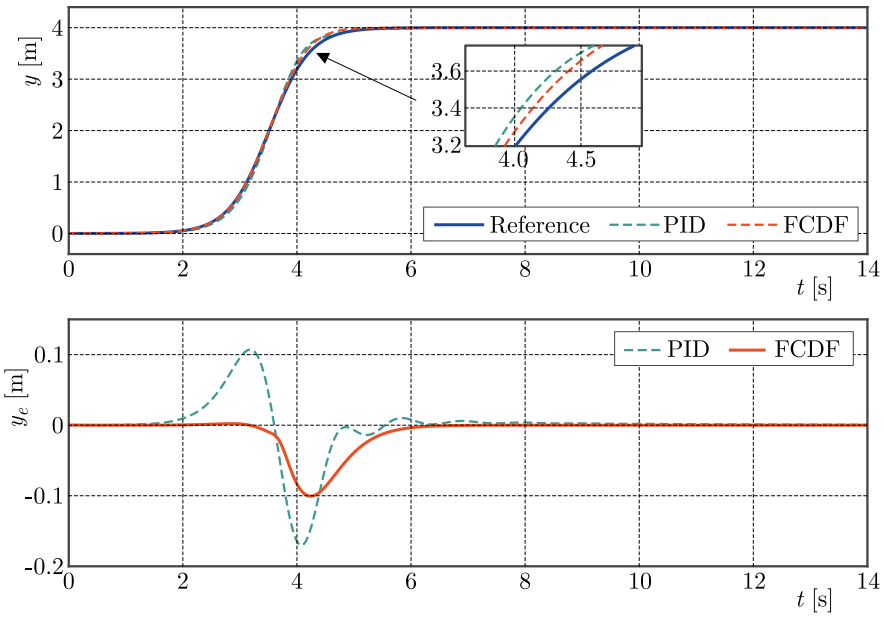

Fig. 5. Trajectory tracking effect and lateral deviation under lane change conditions

Figure 6 shows the yaw angle and its deviation response curve. The maximum yaw angle deviation under FCDF control is within 0.017 rad. The final deviation convergence rate is 1.3 seconds faster than that for PID. The maximum yaw angle deviation for PID control exceeds 0.036 rad, with noticeable oscillations. Figure 7 displays the active steering angle response. The maximum absolute active steering angle for PID and FCDF control is 3.527° and 2.740°, respectively. For PID control, the steering angle oscillation is significant at curve-straight line junctions, potentially causing vehicle instability, while for FCDF control, the steering angle oscillation is slight, ensuring vehicle stability.

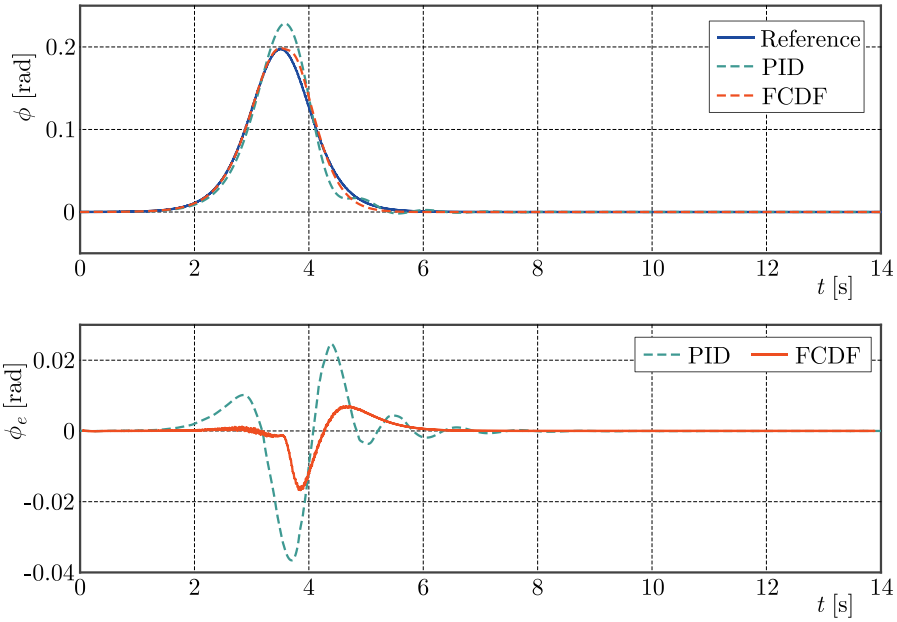

Fig. 6. Yaw angle response and deviation under lane changing conditions

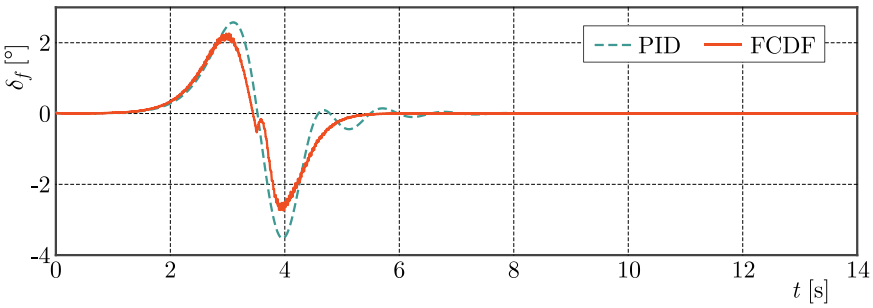

Fig. 7. Active steering angle under lane change condition

For quantitative analysis, the average absolute deviation (ABD), root mean square deviation (RSMDV), and maximum absolute deviation (MBD) were calculated and compared. Table 2 shows that ABD, RSMDV, and MBD are smaller for FCDF compared to PID, indicating better vehicle tracking for FCDF control.

To simulate continuous disturbances during lane changes, a random excitation R_1 is added to the process of obtaining the reference trajectory. The random excitation time in the whole simulation is 14 seconds

$$R_1 = \mu_{r1} + \sigma_{r1} Z_{r1} \tag{5.1}$$

where μ_{r1} represents the mean and its value is 0, σ_{r1} represents the standard deviation and its value is 1, Z_{r1} represents independent and equally distributed random numbers and fol-

Table 2. Comparison of vehicle tracking effects under lane change conditions

Evaluation parameter	Control strategy	ABD	RSMDV	MBD
Lateral displacement [m]	PID	0.0180	0.0411	0.1702
	FCDF	0.0084	0.0240	0.1006
Yaw angle [rad]	PID	0.0031	0.0076	0.0366
	FCDF	0.0010	0.0029	0.0169

lows the normal distribution $N_1(0,1)$, the unit of R_1 is meter, the sampling time is 0.01 seconds; the frequency is 100 Hz.

Figure 8 shows the trajectory tracking and yaw angle response under such conditions. It can be seen that the interference will reduce the vehicle tracking accuracy, increase the yaw angle response and reduce the lateral stability of the vehicle. Despite sustained oscillations and deviations, FCDF control shows better convergence and smaller deviation amplitude compared to PID, demonstrating better robustness against external disturbance.

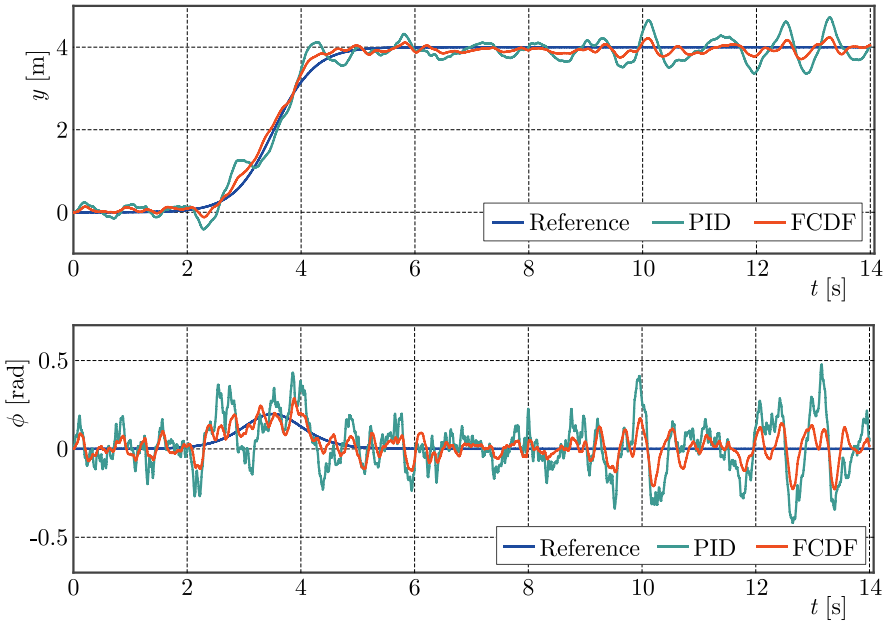

Fig. 8. Trajectory tracking effect and yaw angle response obtained by external random excitation under lane change condition

5.2. Overtaking condition test

This Section verifies the track tracking effect and lateral performance under normal tracking and response performance under external random excitation during overtaking.

Figure 9 shows the trajectory tracking effect and lateral deviation. The maximum lateral deviation for PID and FCDF control is 0.2835 m and 0.1946 m, respectively. FCDF control maintains smaller deviation amplitudes within $(-0.1946,\ 0.0052)$ m. The tracking accuracy is higher in linear sections, with a minimal lateral deviation in curved sections, and the final deviation convergence rate is 2.2 seconds faster than that for PID.

Figure 10 shows the yaw angle deviation response. The maximum yaw angle deviation for FCDF control is within 0.033 rad, with a 3.1 seconds faster convergence to 0 than PID. The maximum deviation for PID control exceeds 0.063 rad, with evident oscillations. Figure 11 shows the active steering angle response. The maximum steering angle for PID and FCDF control is 5.815° and 4.335°, respectively. For PID control, the oscillation amplitude is significant at curve-

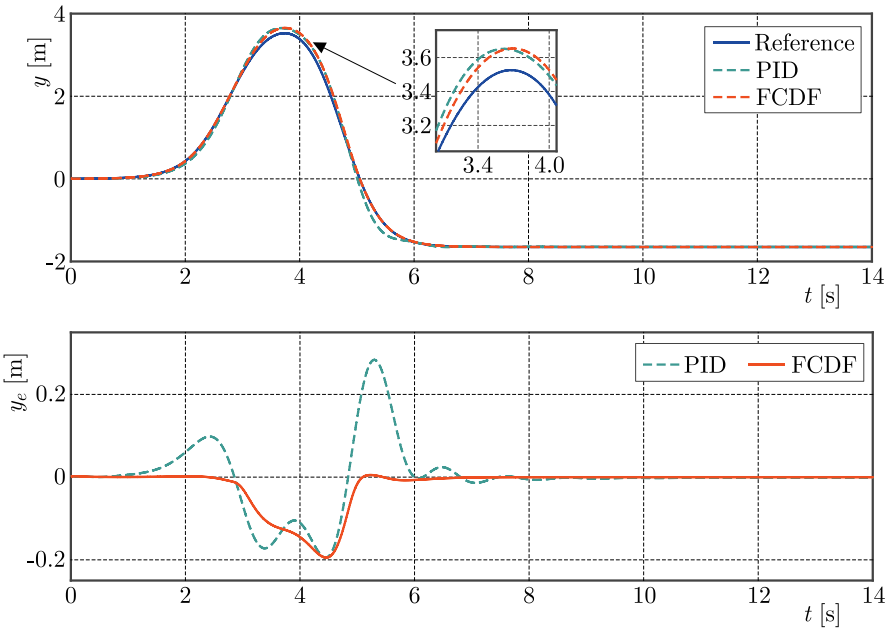

Fig. 9. Trajectory tracking effect and lateral deviation under overtaking conditions

-straight line junctions, risking instability. FCDF control maintains slight oscillations, ensuring stability.

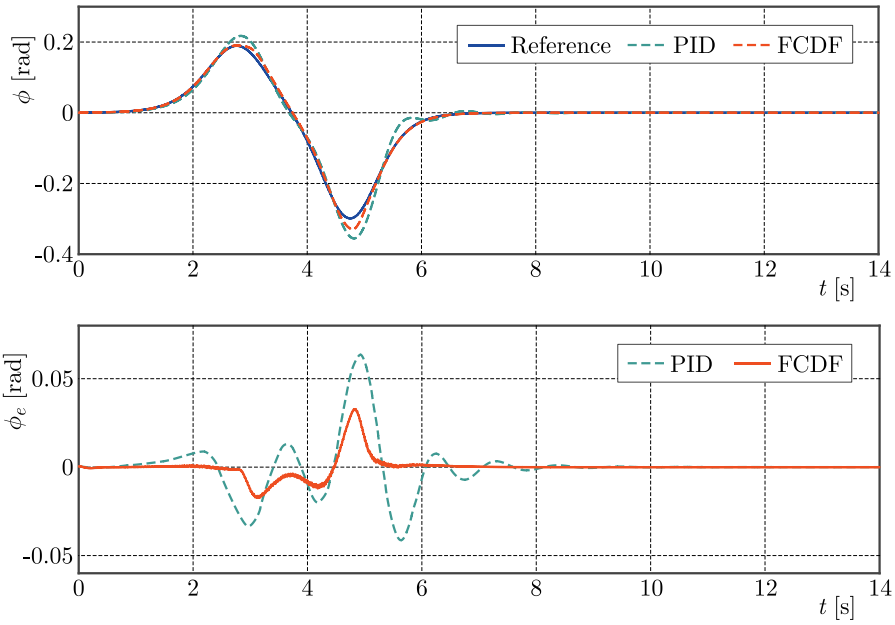

Fig. 10. Yaw angle response and deviation under overtaking conditions

Quantitative analysis (Table 3) of ABD, RSMDV, and MBD shows smaller values for FCDF, indicating better tracking performance than PID. Figure 12 shows that FCDF control has a better convergence and smaller deviation amplitude under external disturbances, demonstrating superior robustness.

Considering the interference of external uncertainties in the system, a random excitation R_2 is added to the process of obtaining the reference trajectory to simulate the change of the system due to continuous disturbance under overtaking conditions. The random excitation time

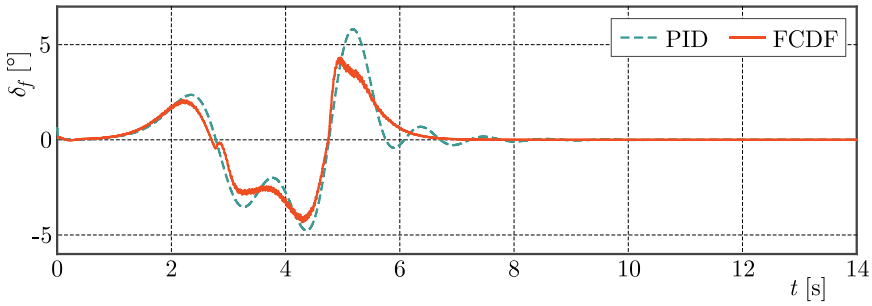

Fig. 11. Active steering angle under overtaking condition

Table 3. Comparison of vehicle tracking effects under overtaking conditions

Evaluation parameter	Control strategy	ABD	RSMDV	MBD
Lateral displacement [m]	PID	0.0427	0.0798	0.2835
	FCDF	0.0207	0.0525	0.1946
Yaw angle [rad]	PID	0.0071	0.0146	0.0636
	FCDF	0.0023	0.0058	0.0328

in the whole simulation is 14 seconds

$$R_2 = u_{r2} + \sigma_{r2} Z_{r2} \tag{5.2}$$

where μ_{r2} represents the mean and its value is 0, σ_{r2} represents the standard deviation and its value is 1, Z_{r2} represents independent and equally distributed random numbers and follows the normal distribution $N_2(0,1)$, the unit of R_2 is meter, the sampling time is 0.01 seconds, the frequency is 100 Hz.

The effect of trajectory tracking and yaw angle response are shown in Fig. 12. It can be seen that the interference will reduce the vehicle tracking accuracy, increase the yaw angle response and reduce the lateral stability of the vehicle. Through intuitive comparative analysis, it can be seen that although the trajectory tracking effect and yaw angle response under the two controllers have sustained oscillation and deviation, the trajectory tracking effect and yaw angle response under the control of FCDF have a better convergence, and the deviation change amplitude is small, and both of them are closer to the reference value. Therefore, compared with PID, FCDF has better robustness to external interference in the trajectory tracking effect and yaw angle response.

According to the comparison of the time-domain response and steady-state response in the simulation test of ASV under different working conditions, FCDF can solve the problem of underdrive in trajectory tracking control better than PID.

5.3. Robustness analysis of FCDF

ASV controller performance is particularly important during path tracking, and ASV is easy to lose stability at high speed. For this reason, the robustness of FCDF was analyzed for different vehicle speeds and road conditions. The reference values corresponding to longitudinal vehicle speeds of 30 km/h, 50 km/h and 90 km/h were Reference 1, Reference 2 and Reference 3, respectively.

Figure 13 shows the comparison of ASV driving conditions at different speeds under lane change conditions. Among them, Fig. 13a reflects the overall effect of ASV trajectory tracking and the lateral deviation generated in the tracking process. Figure 13b reflects the actual yaw response of the ASV and the deviation from the ideal yaw angle. It can be observed from the simulation test results that ASV can maintain a good tracking effect in general, and FCDF

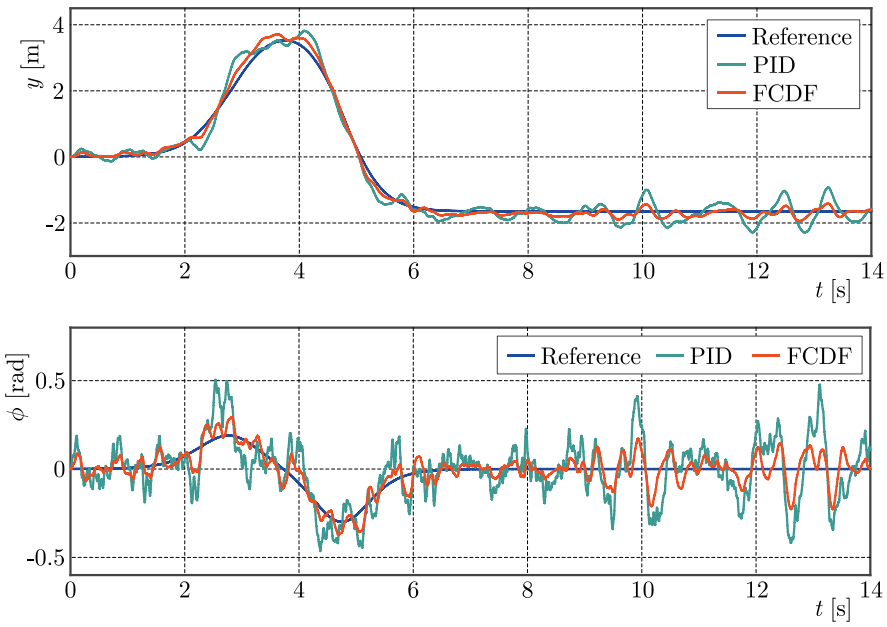

Fig. 12. Trajectory tracking effect and yaw angle response obtained by the external random excitation under the overtaking condition

has good control performance. For the 90 km/h speed test, the trajectory tracking effect and yaw angle response both oscillate slightly during 3 s to 5 s, but their amplitude is small and can converge to 0 quickly. Meanwhile, the lateral deviation and yaw angle deviation in the whole period are kept within a reasonable range.

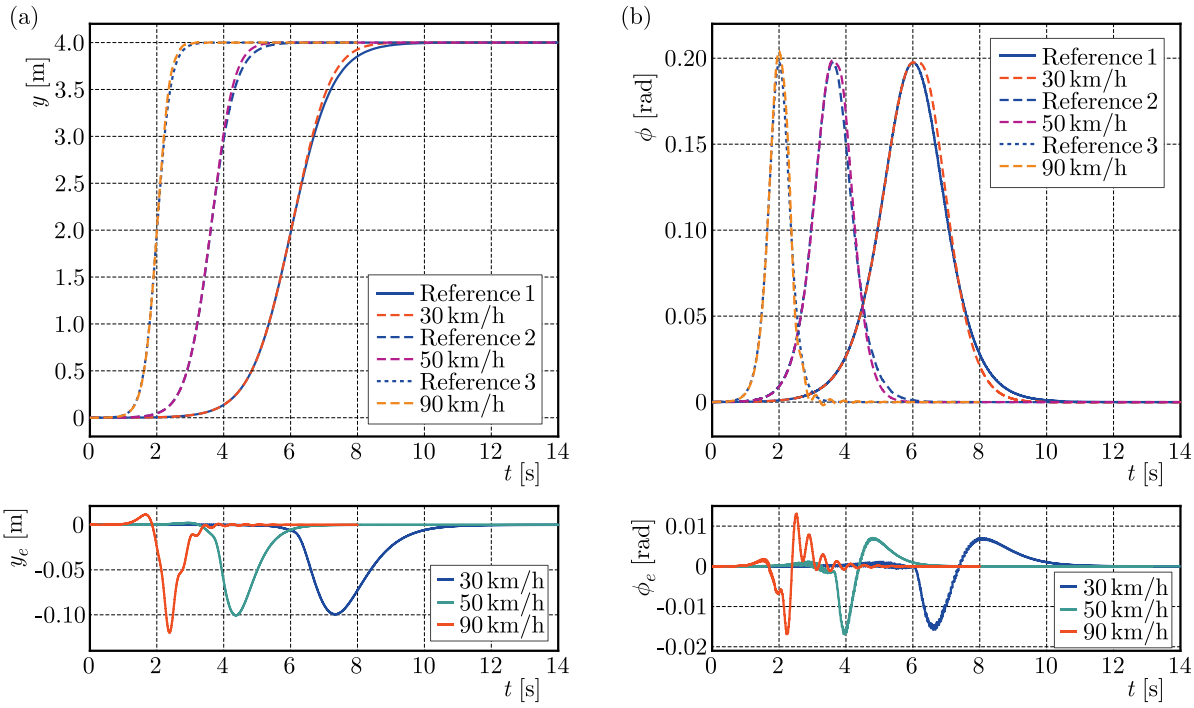

Fig. 13. The control effect of FCDF under different speed in the lane change condition: a) trajectory tracking effect and lateral deviation, b) yaw angle response and deviation

Figure 14 shows the comparison of ASV driving conditions at different speeds under overtaking condition. Among them, Fig. 14a reflects the overall effect of ASV trajectory tracking and

the lateral deviation generated in the tracking process. Fig. 14b reflects the actual yaw response of the ASV and the deviation from the ideal yaw angle. According to the simulation test results, it can be found that a satisfactory tracking effect can be obtained at 30 km/h and 50 km/h, and the transverse deviation and yaw angle deviation values decrease with a decrease of speed. At 90 km/h, high speed and continuous sharp turns adversely affect the lateral stability of the ASV, and the control performance of the FCDF deteriorates, leading to a decline in tracking performance. Especially in the 2 s to 5 s period, the yaw angle oscillation is relatively sharp and the amplitude is large, which may be caused by the side of the vehicle tire, resulting in the tire state touching the nonlinear region.

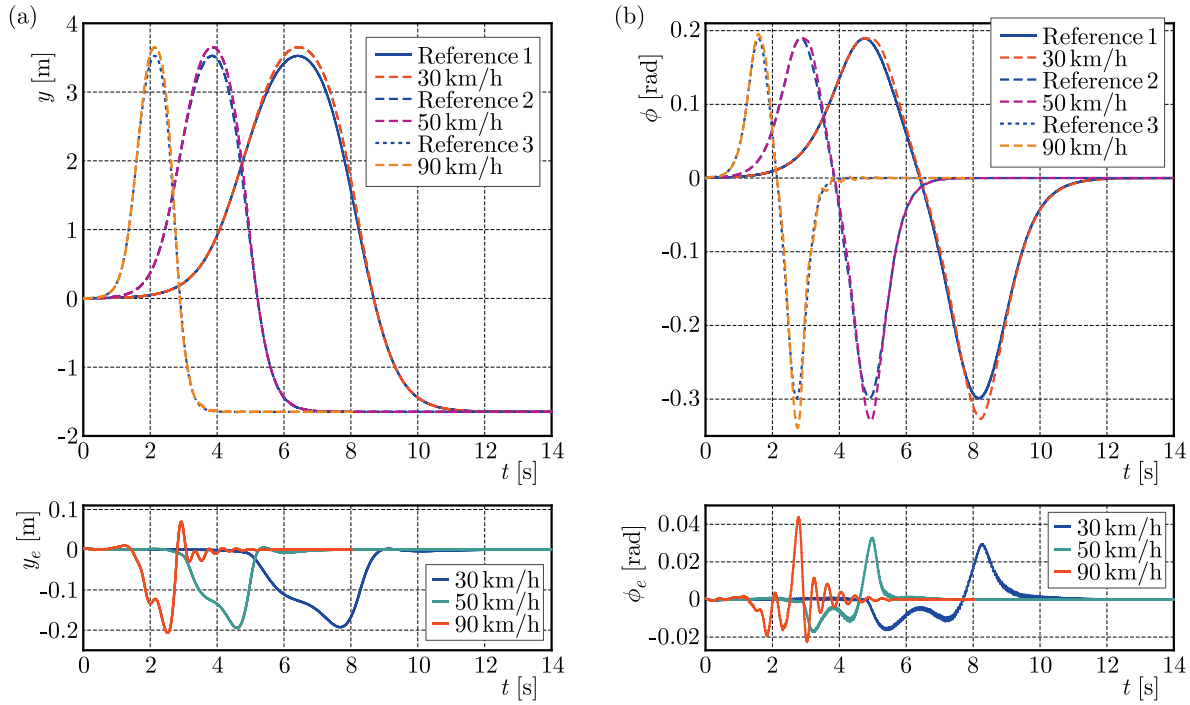

Fig. 14. The control effect of FCDF under different speed in the overtaking condition: a) trajectory tracking effect and lateral deviation, b) yaw angle response and deviation

By comparing the simulation results under different driving conditions and different speeds, the ASV can achieve accurate trajectory tracking and good lateral stability at 30 km/h and 50 km/h speeds, and the control performance of FCDF has good advantages and robustness. As the speed increases to more than 90 km/h, the ASV can achieve reasonable tracking effect in road conditions without continuous sharp turns, while the tracking performance will deteriorate to a certain extent in road conditions with continuous sharp turns. However, as long as the speed is guaranteed to change within the range of 90 km/h, even if there are external disturbances or internal uncertainties worse than the actual situation, the ASV can achieve a reasonable tracking effect in road conditions without continuous sharp turns. The simulation results show that the FCDF controller can still maintain good robustness and the control tracking lateral deviation and yaw angle deviation are bounded, which further shows that the ASV system based on differential flatness theory can effectively solve the underdrive problem.

6. Conclusion

In this paper, based on the active steering vehicle, the trajectory tracking problem of the single-input multi-output vehicle monorail model with an active steering angle input but lateral

displacement and yaw angle output is studied. Firstly, through derivation and application of differential flatness theory, the original vehicle system is transformed into an equivalent form containing only the flat output and its derivatives. Then, the FCDF control strategy is applied to control the vehicle tracking and lateral stability, while dealing with external interference of the system. Finally, the vehicle system was built in Simulink to conduct simulation tests under lane change and overtaking conditions. The simulation results show that the proposed method has certain advantages and is conducive to solving nonlinear and underdrive problems of autonomous vehicles. But the differential flat control method is currently only validated in simulation, and its implementation can be quite complex, requiring an accurate system model and a deep understanding of the system dynamics, and may involve complex calculations. In addition, for systems that do not satisfy differential flatness conditions, other types of control strategies may need to be considered. Our future work will focus on applying the proposed control method to a practical experimental platform.

Acknowledgement

This work was supported in part by the National Natural Science Foundation of China under Grant 52272374 & 52232013, in part by the open project of Key Laboratory of Railway Industry of Maglev Technology.

References

1. Aschemann H., Schindele D., 2008, Sliding-mode control of a high-speed linear axis driven by pneumatic muscle actuators, *IEEE Transactions on Industrial Electronics*, **55**, 11, 3855-3864
2. Bai G.X., Liu L., Meng Y., Luo W.D., Gu Q., Ma B.Q., 2019, Path tracking of mining vehicles based on nonlinear model predictive control, *Applied Sciences*, **9**, 7, 1372
3. Elmi N., Ohadi A., Samadi B., 2013, Active front-steering control of a sport utility vehicle using a robust linear quadratic regulator method, with emphasis on the roll dynamics, *Proceedings of the Institution of Mechanical Engineers, Part D: Journal of Automobile Engineering*, **227**, 12, 1636-1649
4. Fliess M., Lévine J., Martin P., Rouchon P., 1995, Flatness and defect of non-linear systems: Introductory theory and examples, *International Journal of Control*, **61**, 6, 1327-1361
5. Guerrero J., Chemori A., Torres J., Creuze V., 2023, Time-delay high-order sliding mode control for trajectory tracking of autonomous underwater vehicles under disturbances, *Ocean Engineering*, **268**, 113375
6. Huang C.Z., Luo C.M., Li Y., Zhang T.Y., 2019, Differential flatness active disturbance rejection control approach for a class of nonlinear uncertain systems, *International Journal of Robotics and Automation*, **34**, 2, 146-155
7. Kang N., Han Y., Guan T., Wang S., 2022, Improved ADRC-based autonomous vehicle path-tracking control study considering lateral stability, *Applied Sciences*, **12**, 9, 4660
8. Li Z., Li J., Wang W., 2023, Path planning and obstacle avoidance control for autonomous multi-axis distributed vehicle based on dynamic constraints, *IEEE Transactions on Vehicular Technology*, **72**, 4, 4342-4356
9. Luo L., Cao S.Y., Sheng Z., Shen H.L., 2022, LiDAR-based global localization using histogram of orientations of principal normals, *IEEE Transactions on Intelligent Vehicles*, **7**, 3, 771-782
10. Mata S., Zubizarreta A., Pinto C., 2019, Robust tube-based model predictive control for lateral path tracking, *IEEE Transactions on Intelligent Vehicles*, **4**, 4, 569-577
11. Menhour L., d'Andréa-Novel B., Fliess M., Mounier H., 2014, Coupled nonlinear vehicle control: Flatness-based setting with algebraic estimation techniques, *Control Engineering Practice*, **22**, 135-146

12. Ortiz F.M., Sammarco M., Costa L.H.M., Detyniecki M., 2023, Applications and services using vehicular exteroceptive sensors: A survey, *IEEE Transactions on Intelligent Vehicles*, **8**, 1, 949-969

13. Rokonuzzaman M., Mohajer N., Nahavandi S., Mohamed S., 2021, Model predictive control with learned vehicle dynamics for autonomous vehicle path tracking, *IEEE Access*, **9**, 128233-128249

14. Sira-Ramirez H., Agrawal S.K., 2018, *Differentially Flat Systems*, CRC Press

15. Sun Y.G., He Z.Y., Xu J.Q., Sun W., Lin G.B., 2023, Dynamic analysis and vibration control for a maglev vehicle-guideway coupling system with experimental verification, *Mechanical Systems and Signal Processing*, **188**, 109954

16. Sun Y.G., Li F.X., Lin G.B., He Z.Y., 2023, Adaptive fault-tolerant control of high-speed maglev train suspension system with partial actuator failure: design and experiments, *Journal of Zhejiang University-SCIENCE A*, **24**, 3, 272-283

17. Sun Y.G., Qiang H.Y., Wang L., Ji W., Mardani A., 2023, A fuzzy-logic-system-based cooperative control for the multielectromagnets suspension system of maglev trains with experimental verification, *IEEE Transactions on Fuzzy Systems*, **31**, 10, 3411-3422

18. Sun Z.Y., Wang R.C., Meng X.P., Yang Y.Y., Wei Z.D., Ye Q., 2024, A novel path tracking system for autonomous vehicle based on model predictive control, *Journal of Mechanical Science and Technology*, **38**, 1, 365-378

19. Wang R.R., Zhang H., Wang J.M., 2014, Linear parameter-varying controller design for four-wheel independently actuated electric ground vehicles with active steering systems, *IEEE Transactions on Control Systems Technology*, **22**, 4, 1281-1296

20. Wang X., Sun W.C., 2023, Trajectory tracking of autonomous vehicle: A differential flatness approach with disturbance-observer-based control, *IEEE Transactions on Intelligent Vehicles*, **8**, 2, 1368-1379

21. Wang Z.Q., Sun K.Y., Ma S.Q., Sun L.T., Gao W., Dong Z.Z., 2022, Improved linear quadratic regulator lateral path tracking approach based on a real-time updated algorithm with fuzzy control and cosine similarity for autonomous vehicles, *Electronics*, **11**, 22, 3703

22. Xia Y.Q., Pu F., Li S.F., Gao Y., 2016, Lateral path tracking control of autonomous land vehicle based on ADRC and differential flatness, *IEEE Transactions on Industrial Electronics*, **63**, 5, 3091-3099

23. Yang T., Bai Z.W., Li Z.Q., Feng N.L., Chen L.Q., 2021, Intelligent vehicle lateral control method based on feedforward + predictive LQR algorithm, *Actuators*, **10**, 9, 228

24. Yu H.W., Zhang Z.Z., Xing J.F., 2021, Micro feed characteristic analysis of a new crawler guide rail dual drive servo system, *Science Progress*, **104**, 3, 1-24

25. Zhuang Y.F., Ma G.F., Huang H.B., 2010, Time-optimal motion planning of an underactuated rigid spacecraft, *Control and Decision* (in Chinese), **25**, 10, 1469-1473

Manuscript received July 14, 2024; accepted for publication November 8, 2024